Published in final edited form as:
Biomaterials. 2010 June ; 31(18): 4926–4934. doi:10.1016/j.biomaterials.2010.03.001.

Regulating *in vivo* calcification of alginate microbeads

Christopher S.D. Lee[a], **Hunter R. Moyer**[b,c], **Rolando A. Gittens I.**[d], **Joseph K. Williams**[c], **Adele L. Boskey**[e,f], **Barbara D. Boyan**[a,*], and **Zvi Schwartz**[a,g]

[a]Wallace H. Coulter Department of Biomedical Engineering and Institute for Bioengineering and Bioscience, Georgia Institute of Technology, 315 Ferst Drive NW, Atlanta, GA 30332-0363, Atlanta, GA, USA

[b]Division of Plastic and Reconstructive Surgery, Department of Surgery, Emory University Medical School, Atlanta, GA, USA

[c]Children's Healthcare of Atlanta, Atlanta, GA, USA

[d]School of Materials Science and Engineering, Georgia Institute of Technology, Atlanta, GA, USA

[e]Research Division, Hospital for Special Surgery, New York, NY, USA

[f]Departments of Biochemistry and of Physiology, Biophysics and Systems Biology, Weill Medical College of Cornell University, New York, NY, USA

[g]Department of Periodontics, University of Texas Health Science Center at San Antonio, San Antonio, TX, USA

Abstract

Alginate calcification has been previously reported clinically and during animal implantation; however no study has investigated the mechanism, extensively characterized the mineral, or evaluated multiple methods to regulate or eliminate mineralization. In the present study, alginate calcification was first studied *in vitro*: calcium-crosslinked alginate beads sequestered surrounding phosphate while forming traces of hydroxyapatite. Calcification *in vivo* was then examined in nude mice using alginate microbeads with and without adipose stem cells (ASCs). Variables included the delivery method, site of delivery, sex of the animal, time *in vivo*, crosslinking solution, and method of storage prior to delivery. Calcium-crosslinked alginate microbeads mineralized when injected subcutaneously or implanted intramuscularly after 1–6 months. More extensive analysis with histology, microCT, FTIR, XRD, and EDS showed calcium phosphate deposits throughout the microbeads with surface mineralization that closely matched hydroxyapatite found in bone. Incorporating 25 mM bisphosphonate reduced alginate calcification whereas using barium chloride eliminated mineralization. Buffering the crosslinking solution with HEPES at pH 7.3 while washing and storing samples in basal media prior to implantation also eliminated calcification *in vivo*. This study shows that alginate processing prior to implantation can significantly influence bulk hydroxyapatite formation and presents a method to regulate alginate calcification.

Keywords

Calcification; Alginate; Microencapsulation; Adipose stem cell microbeads; Bone tissue engineering

*Corresponding author. Tel.: +1 404 385 4108; fax: +1 404 894 2291. barbara.boyan@bme.gatech.edu (B.D. Boyan).

1. Introduction

Alginate hydrogels have been used for a wide variety of tissue engineering and regenerative medicine applications because they have favorable mass transfer properties [1], can be molded into specific shapes [2,3], have adjustable degradation kinetics [4–6], support a range of different cell phenotypes [7–9], can be mechanically and biochemically modified [10–12], support cell differentiation in large animal models [13], and are biocompatible for delivery of cells in human trials [14]. The most common method of incorporating bioactive molecules or cells into alginate matrices is via extrusion, in which an alginate suspension is extruded through a needle to form droplets that fall into a solution that contains divalent cations causing alginate crosslinking [8,15–17]. Alginate microspheres can also be created by using air flow [18] or high electrostatic potentials [19] to overcome surface tension, and have been used to encapsulate and deliver pancreatic islets [8]. In addition to cell delivery, hydrogel microspheres have generally been used for spheroid cell culture, drug delivery, and as injec tissue fillers. The ability of alginate microspheres as an injectable filler to deliver encapsulated cells has not been fully characterized, and, to further develop this technology, the mass transfer properties and reabsorption kinetics of alginate microspheres must be controllable *in vivo*.

Various pre-clinical and clinical studies have reported alginate calcification [20–22], which presents a critical challenge in developing large scale applications using this hydrogel. Our preliminary studies have shown that alginate microbeads calcify *in vivo*, which affects mass transfer in and out of the hydrogel while preventing reabsorption and creating unwanted mineralization foci within the tissue. Therefore, it would be advantageous to develop methods to prevent alginate calcification. However, if alginate calcification can be regulated temporally and spatially *in vivo*, this hydrogel could also be used as a stimulus for *in situ* bone repair and formation. To achieve this type of application, a thorough understanding of the mechanism of alginate calcification and methods to control it need to be developed. No study, however, has yet extensively characterized alginate calcification nor has any study thoroughly investigated methods to control this process.

The objective of this study was to investigate how alginate beads calcify and to develop different methods to control alginate calcification while characterizing the mineral formed. We first hypothesized that calcium-crosslinked alginate calcifies by sequestering the surrounding phosphate to form calcium phosphate. Alginate beads were cultured in a phosphate solution, and phosphate content and subsequent mineralization were analyzed. We then hypothesized that calcium-crosslinked alginate has the ability to calcify *in vivo* regardless of the presence of encapsulated cells, delivery method, site of delivery, or sex of the animal. Alginate microbeads seeded with or without human adipose stem cells were implanted intra-muscularly or injected subcutaneously in male and female nude mice and the retrieved implants analyzed for mineral content and properties. Finally, we hypothesized that the type of mineral would be similar to hydroxyapatite found in bone and that this calcification could be eliminated by varying divalent cations used to crosslink alginate or by buffering the pH in the beads before implantation. Barium was used as a crosslinking ion since it does not readily interact with phosphate ions [23] whereas alendronate was added since it is a bisphosphonate that chelates calcium and attaches strongly to hydroxyapatite to prevent crystal growth [24]. HEPES, an organic zwitterion buffering agent that does not contain phosphate, was used to buffer the crosslinking bath below physiological levels since hydroxyapatite crystals are stable to neutral to alkaline environments [25]. Implanted alginate microbeads created in different crosslinking solutions were retrieved and extensively characterized.

2. Materials and methods

2.1. In vitro phosphorus content

To test our first hypothesis that calcium-crosslinked alginate calcifies by sequestering surrounding phosphate, an *in vitro* study was designed to assess the ability of calcium-crosslinked alginate to sequester phosphate. Low viscosity sodium alginate [Kelco Corp., Chicago, IL, USA] dissolved in 155 mM sodium chloride at a concentration of 12 mg/ml was dropped gently through a 25 gauge needle at a rate of 2–3 drops per second into a 102 mM calcium chloride bath. After 10 min, the beads (15–20 beads/10 ml alginate) were washed four times with 155 mM NaCl. The beads were suspended in 25 ml 4 mM $(NH_4)_2HPO_4$ in 0.05 M Tris buffer at pH 7.4, and removed at different time points over a 4 h period (0, 0.5, 1, 2, and 4 h). After incubation at room temperature, the beads were collected by centrifugation, and the supernatants were assayed for phosphorus content using a commercially available kit [Sigma, St. Louis, MO, USA] ($n = 3$ for each experimental group and time). Beads were then lyophilized, mixed with KBr (~1 wt%), and made into KBr pellets for Fourier transform infrared spectroscopy (FTIR) analysis as outlined below. In some cases, the cloudy supernatant of the incubation buffer was centrifuged to a pellet, washed with acetone, air dried, and analyzed as a KBr pellet via FTIR.

2.2. Cell isolation and culture

To test our second hypothesis that calcium-crosslinked alginate microbeads with and without cells would calcify *in vivo*, adipose stem cells (ASCs) were isolated. Fat was excised from male and female patients less than 18 years of age undergoing cosmetic and reconstructive procedures at Children's Healthcare of Atlanta under an approved IRB protocol at Georgia Institute of Technology and Children's Healthcare of Atlanta. All patients and parents gave written consent to both the procedure and handling of fat thereafter. ASCs were isolated via a collagenase digestion solution as previously described [26]. Cells were then seeded at 5000 cells/cm^2 and cultured in Lonza Mesenchymal Stem Cell Growth Medium [Lonza, Basel, Switzerland] up to second passage.

2.3. Alginate bead and microbead fabrication

To test our hypotheses that alginate calcification can occur independently of how and where microbeads were implanted and that it could be eliminated by varying the crosslinking method, alginate microbeads were made in different crosslinking solutions. Medium molecular weight alginate (240,000 kDa) with a high guluronate to mannuronate ratio (69% guluronate) [FMC Biopolymer, Drammen, Norway] was UV light sterilized and dissolved in 155 mM sodium chloride [Ricca Chemical, Arlington, TX, USA] at a concentration of 20 mg/ml. Alginate containing ASCs was initially seeded at 1×10^6 cells/ml, resulting in a final measured cell number of 40 ± 7 cells per microbead (Fig. 2B). Microspheres were created using a Nisco Encapsulator VAR V1 LIN-0043 [Nisco Engineering AG, Zurich, Swizterland] at a 4 ml/h flow rate, 0.175 mm nozzle inner diameter, and 6 kV electrostatic potential [27]. Microbeads were made in four different crosslinking solutions: (i) 50 mM $CaCl_2$ and 150 mM glucose (non-buffered); (ii) 50 mM $CaCl_2$ and 150 mM glucose with 25 mM alendronate [Sigma] (bisphosphonate); (iii) 20 mM $BaCl_2$ and 150 mM glucose (barium); and (iv) 50 mM $CaCl_2$ and 150 mM glucose with 15 mM 4-(2-hydroxyethyl)-1-piperazineethanesulfonic acid at pH 7.3 [Sigma] (HEPES-buffered). Microbeads made in non-buffered crosslinking solutions were washed and stored in 155 mM sodium chloride (saline) while microbeads made in the HEPES-buffered crosslinking solution were washed and stored in Dulbecco's modified eagle medium (DMEM) [Invitrogen, Carlsbad, CA, USA] at 37 °C and 5% CO_2 prior to implantation to allow for longer term storage of ASC microbeads in future studies. Following microencapsulation, microbeads were implanted as described below.

2.4. Cell viability

To determine whether ASCs were viable after microencapsulation in alginate and remained viable after injection delivery, microencapsulated ASCs suspended in DMEM were injected as described below and cultured for 0, 1, and 2 weeks in Lonza Mesenchymal Stem Cell Growth Medium. Microencapsulated ASCs that were not injected were also cultured for comparison ($n = 6$ for each experimental group and time). Viability was measured using fluorescent confocal microscopy using a LIVE/DEAD Viability Kit following the manufacturer's protocol [Invitrogen]. Briefly, samples were incubated for 30 min in a PBS solution containing 10 mM $CaCl_2$, 4 mM ethidium homodimer-1, and 2 mM calcein and imaged with a LSM 510 confocal microscope [Carl Zeiss MicroImaging Inc., Thornwood, NY].

2.5. Animal surgeries

Male and female athymic nude (Nu/Nu) mice were housed in the vivarium in the Institute for Bioengineering and Bioscience at the Georgia Institute of Technology and handled under a protocol approved by the IACUC committee. Prior to surgeries, athymic mice were anesthetized using isoflurane gas. Both non-buffered and HEPES-buffered microbeads were directly implanted subcutaneously or intramuscularly or injected subcutaneously to determine if delivery method affected alginate calcification. Bisphosphonate and barium microbeads were only injected subcutaneously to reduce animal discomfort and to investigate how the crosslinking solution affects alginate calcification. For intramuscular implants, a small skin incision was made over the calf region of the hind limb, a pouch was prepared in the muscle by blunt dissection, and approximately 0.1 ml microbeads were inserted directly into the gastrocnemius muscle [28]. For all subcutaneous injections, 0.25 ml microbeads were mixed in 0.25 ml DMEM and injected via an 18 gauge needle. Animals were euthanized by CO_2 inhalation at various time points from 1 to 6 months. Each animal received either 2 injections or 2 implantations subcutaneously or 2 bilateral intramuscular implantations ($n = 4–6$ for each experimental condition). Samples were harvested and processed for subsequent studies as described below.

2.6. Micro-computed tomography

To assess the extent of alginate microbead mineralization, subcutaneous and intramuscular samples were excised from nude mice, immediately scanned using a μCT 40 (Scanco Medical, Switzerland) with a voxel size of 20 μm, and analyzed as previously described [29]. Calcification was identified using a fixed threshold; individual samples were isolated with user-guided contours and three-dimensional images were created. Samples were then fixed in 10% neutral buffered formalin [Sigma] for histological processing or frozen and lyophilized for subsequent materials characterization.

2.7. Histology

After 48 h of fixation in formalin, representative undecalcified samples were embedded in plastic, and cut into 10-μm thick sections. Samples were stained with von Kossa with a nuclear fast red counter stain as previously described [30].

2.8. Fourier transform-infrared spectroscopy (FTIR)

To test our hypothesis that alginate calcification mineral was similar to hydroxyapatite found in bone, infrared spectroscopy in attenuated total internal reflection (ATR) mode [Pike Technologies, Madison, WI, USA] was performed on lyophilized samples using a Nexus 870 FTIR bench [Nicolet Instrument Corporation, Madison, WI, USA]. Each spectrum was the mean of two acquisitions (between 1800 and 800 cm^{-1}) of at least 64 scans with a spectral resolution of 4 cm^{-1}.

2.9. X-ray diffraction

Crystal structure of the samples was identified using an X'Pert PRO Alpha-1 diffractometer [PANalytical, Almelo, The Netherlands]. X-ray diffraction (XRD) scans were collected using Cu Kα radiation. A 1° parallel plate collimator, ½ divergence slit and 0.04 rad soller slit were used for controlled axial divergence. Bragg–Brentano parafocusing at 45 kV and 40 mA was used to analyze samples. The assignment of detected peaks to crystalline phases was performed using the database from the International Centre for Diffraction Data (ICDD, 2008).

2.10. Scanning electron microscopy and energy dispersive X-ray spectroscopy

Morphology of the microbeads was qualitatively evaluated using an Ultra 60 field emission scanning electron microscope (FESEM) [Carl Zeiss SMT Ltd., Cambridge, UK] at an accelerating voltage of 5 kV and different magnifications. Chemical composition of samples was determined using an INCAPentaFET-x3 energy dispersive X-ray spectrometer (EDS) [Oxford Instruments, Bucks, UK] at an accelerating voltage of 15 kV and a working distance of 8.5 mm.

3. Results

3.1. In vitro calcification

Upon adding the calcium-crosslinked alginate beads to the phosphate buffer, the solution started to become cloudy. The phosphate concentration in the bath decreased by 20–35% over the first 4 h and depended on the amount of alginate that was added (Fig. 1A). The FTIR spectrum of the lyophilized alginate had peaks between 1600 and 1800 cm^{-1}, 1370–1525 cm^{-1}, and 900–1200 cm^{-1} (Fig. 1B) while the FTIR spectrum of the phosphate bath pellet had a similar peak between 900 and 1200 cm^{-1} along with peaks centered around 1600 and 1400 cm^{-1} (Fig. 1C). Pure hydroxyapatite had characteristic peaks between 1400 and 1550 cm^{-1} and 900–1200 cm^{-1} (Fig. 1D).

3.2. Visualization of in vivo calcification

Microbeads formed in all crosslinking solutions ranged from 200 to 350 mm in diameter (Fig. 2A). When non-buffered microbeads were either implanted or injected subcutaneously into male nude mice, almost every sample showed the presence of mineral at all time points examined (1, 3, and 6 months; Table 1). Specifically, 24 of 24 implanted samples calcified whereas 21 of 24 injected samples calcified. ASC viability prior to implantation or injection was 70 ± 3% (Fig. 2B), and *in vitro* studies show cell viability increasing to 80 ± 5% two weeks post-injection (data not shown), yet the presence of ASCs had no apparent effect on mineralization (Table 1). Mineralization was demonstrated by light microscopy (Fig. 2C) or by visual inspection of implanted (Fig. 2D) and injected (Fig. 2E) microbeads.

Modifications to the crosslinking protocol reduced or eliminated calcification as detected by von Kossa staining (Table 2). When microbeads were injected subcutaneously, no visual calcification was evident when barium chloride was used as the crosslinker and the addition of the 25 mM bisphosphonate to the crosslinking solution partially reduced mineralization. HEPES-buffered (pH 7.3) microbeads injected subcutaneously also had no apparent calcification. When HEPES-buffered samples were then directly implanted subcutaneously and intramuscularly, there was no visual mineralization. In contrast, when non-buffered microbeads were implanted a second time, all the subcutaneous and two-thirds of the intramuscular samples mineralized.

The intensity of von Kossa staining for phosphate was very strong in non-buffered samples as phosphate was present throughout almost every microbead (Fig. 3A). Barium chloride-

treated samples had no detectable presence of von Kossa staining with microbeads surrounded by endothelial tissue (Fig. 3B). Bisphosphonate-treated samples that did calcify only had partially positive staining for phosphate as both the intensity of staining and the number of positively stained microbeads was lower compared to non-buffered samples (Fig. 3C, Table 2). HEPES-buffered samples had no von Kossa staining and were surrounded by connective tissue (Fig. 3D).

Cross-sectional X-ray sections of non-buffered samples via microCT showed extensive mineralization that was not just limited to the surfaces of individual microbeads or peripheral microbeads of the bolus (Fig. 4A and B). Additionally, the intensity of X-ray attenuation seemed to be comparable to the adjacent bone. 3-D reconstructions further demonstrate the extent of calcification of both subcutaneous (Fig. 4C) and intramuscular (Fig. 4D) samples. HEPES-buffered samples were undetectable by microCT (data not shown).

3.3. Characterization of in vivo calcification

Comparison of FTIR spectra of the lyophilized explanted samples presented significant differences. The spectrum of the non-buffered sample (Fig. 5A) showed the characteristic bands of hydroxyapatite around 1400–1550 cm^{-1} and 900–1200 cm^{-1} and corresponded well with the spectrum of the pure hydroxyapatite powder. The spectrum of the HEPES-buffered sample (Fig. 5B) had no traces of the HEPES spectrum (Fig. 5C), but matched almost perfectly with the spectrum of the pure alginate powder (Fig. 5D). No presence of hydroxyapatite was noted in the HEPES-buffered sample.

The XRD spectra of the explanted samples showed the presence of monphasic crystalline structures (Fig. 6). The alginate powder presented no diffraction pattern. The non-buffered sample appeared to have the crystal structure of hydroxyapatite, whereas the HEPES-buffered sample showed the main peaks of NaCl crystals and incorporated none of the peaks of the HEPES buffer. The crystalline structures were further confirmed with the EDS spectra (Table 3), which showed the presence of 10.2 ± 1.3% Ca and 6.3 ± 0.8% P on the non-buffered sample (Ca/P ratio of 1.6 ± 0.4), and only approximately 1% of each on the HEPES-buffered sample. Conversely, the HEPES-buffered sample included 14.3 ± 0.7% Na and 13.2 ± 1.8% Cl, and the non-buffered sample had <1% of Na and no traces of Cl. The main components of both samples were C and O, primarily from the alginate polymer. SEM image of non-buffered microbeads that were lyophilized shows an intact spherical structure with surrounding tissue growth (Fig. 7A) whereas HEPES-buffered microbeads that were lyophilized were clearly fragmented (Fig. 7B).

4. Discussion

Alginate mineralization has been sporadically reported when used for biomedical research and clinical applications [20–22]. The presence of such calcifications hinders soft tissue regeneration; therefore, effective strategies are needed to eliminate alginate calcification. This study is the first to characterize the mineralization that occurs, propose a mechanism behind alginate calcification, and develop strategies to modulate alginate calcification. It appears that alginate calcification both *in vitro* and *in vivo* occurs due to the alginate hydrogel providing a bolus of calcium ions that then interacts with surrounding phosphate ions to form calcium phosphate salts. This finding is confirmed by our *in vitro* results in which phosphate is sequestered from the solution into the alginate and by our *in vivo* results where alginate crosslinked with barium – a divalent cation that does not readily interact with phosphate ions [23] – exhibited no mineralization, and the addition of alendronate – a bisphosphonate that prevents crystal growth at concentrations as low as 10^{-6} M [24] – reduced calcification. Although barium was effective at preventing calcification, it is known

to be toxic at high levels [31] and hinders the ability for alginate to reabsorb while it significantly retards the delivery of soluble proteins [23]. Despite the alendronate's partial effectiveness, bisphosphonates are known to have a wide variety of side effects when treating osteoporosis [32] and have been shown to influence differentiation of stem cells [33]. Therefore, another method of regulating calcification induced by the alginate beads was investigated.

Hydroxyapatite crystals are stable to neutral to alkaline environments [25]. Therefore it was believed that buffering the pH of alginate hydrogels slightly below physiological levels with a non-phosphate buffer would help eliminate calcification *in vivo* while minimizing any biological side effects. HEPES was selected because it does not contain phosphate, is commonly used in cell culture, and is also effective for maintaining enzyme structure and function below physiological temperatures [34]. Additionally, instead of washing and storing microbeads in saline, which is the standard care for most medical implants, DMEM was used to allow for longer term storage of microbeads with encapsulated cells. MicroCT imaging along with von Kossa staining of precipitated phosphate showed extensive mineralization of non-buffered and saline-stored samples whereas buffering with HEPES and maintaining the pH of the crosslinking solution to pH 7.3, along with washing and storing samples in DMEM, completely eliminated mineralization. Both microCT and histology showed that calcification was not limited to just the surface, suggesting that the calcium crosslinks throughout the microbeads play a major role in alginate calcification.

Further investigation using FTIR, XRD, and EDS showed that hydroxyapatite is the most stable crystal phase formed when alginate is calcified. Explanted non-buffered alginate microbeads had similar spectra to pure hydroxyapatite for both FTIR and XRD whereas buffered microbeads appeared to be a combination of alginate powder and salt crystals when both analytical modalities were used. Specifically, FTIR spectrum of non-buffered microbeads closely resembled that of 16-day-old rat calvaria with characteristic phosphate (900–1180 cm^{-1}) and amide I (1580–1750 cm^{-1}) peaks [35]. Although, the broad phosphate peak in the non-buffered microbeads does overlap with aryl-hydroxyl (1030–1085 cm^{-1}) and carboxylic acid (915–995 cm^{-1}) groups found in the HEPES-buffered microbeads and alginate powder, the disappearance of alginate peaks found at lower frequencies, the low intensities of the amide I and II peaks (1405–1420, 1600–1690 cm^{-1}) in the non-buffered samples, and the XRD spectra suggest the formation of hydroxyapatite. To confirm these findings, the Ca/P ratio for non-buffered alginate was found to be 1.6 ± 0.4, which closely matches hydroxyapatite found in bone [36]. Non-buffered microbeads also had traces of Mg, which has been associated with facilitating the formation of calcified pathological cardiovascular deposits [37]. HEPES-buffered microbeads only had traces of calcium left, suggesting that these samples were starting to be reabsorbed. The presence of sulfur and higher content of carbon in HEPES-buffered microbeads compared to non-buffered samples suggest levels of tissue incorporation, which was also confirmed with histology. More studies though are needed to determine the ability of injectable microbeads to be used for tissue replacement or regeneration.

Cell-mediated mineralization is a complex process, and it is probable that multiple factors contribute to alginate calcification and its inhibition. It is not completely clear why buffering the calcium chloride bath with HEPES at a pH slightly below physiological levels (7.3) or washing and storing alginate microbeads in basal DMEM would prevent mineralization. Hydroxyapatite does not form de novo at pH less than 6.8 [25]. More soluble calcium phosphate phases form at lower pH values, hence the kinetics for hydroxyapatite mineral deposition would be lessened at the lower pH. It is possible that washing and storing microbeads in DMEM may have deposited amino acids such as glutamine or lysine that inhibited growth of any hydroxyapatite nuclei in a similar manner to how salivary proteins

in supersaturated saliva prevent calcium phosphate mineral precipitation by adsorbing active sites of crystallite surfaces [25]. However, this explanation does not explain why non-buffered microbeads that were injected in DMEM still calcified. It is likely that making microbeads in HEPES-buffered calcium chloride at this lower pH and subsequent washing and storage in media was more effective than non-buffered saline alone in removing excess calcium ions and preventing hydroxyapatite nuclei from forming. Additionally, it has been shown that HEPES binds calcium ions with a maximum apparent binding of 1.24 ± 0.001 mmol of Ca^{2+}/L by HEPES at 10 mM and pH 7.39 [38].

Although alginate microbead calcification did not strongly depend on the delivery method, delivery site, the presence of cells, or sex of the animal, biological factors can play a significant role in mineralizing alginate constructs *in vivo*. When bone marrow mesenchymal stem cells (MSCs) were treated with 10^{-7} dexamethasone and 10 ng/ml TGF-b1 for more than 1 week, these cells were able to mineralize alginate scaffolds *in vivo* whereas scaffolds with cells treated for only 1 day had no apparent calcification [21]. Osteogenic-induced adipose stem cells are able to calcify collagen scaffolds both *in vitro* and subcutaneously [39], and alginate microbeads containing a combination of osteoprogenitor and endothelial cells have been shown to mineralize in a metaphyseal femoral bone defect [40]. The final adipose stem cells concentration in our alginate microbeads is similar to MSC-seeded alginate constructs in Ma et al (2×10^6 cells/ml) [21] but significantly less than the microencapsulated osteoprogenitor and endothelial cells in Grellier et al (20×10^6 cells/ml) [40]. Regardless, to better use alginate microbeads for different tissue engineering strategies, more studies are needed to understand the exact mechanisms regulating *in vivo* mineralization of alginate.

Natural biomineralization systems and previous *in vitro* experiments have suggested that crystal nucleation and growth from organic templates occurs on surfaces that expose repetitive patterns of anionic groups [36,41]. These negatively charged groups concentrate and create local supersaturation of inorganic cations, which leads to oriented nucleation of crystal formation. Alginate is a co-polymer with negatively charged blocks of (1–4)-linked β-D-mannuronate and (1–4)-linked α-L-guluronate residues. This structure may allow alginate polysaccharide chains to facilitate controlled calcification for bone tissue engineering. Peptide-amphiphile nanofibers modified with negatively charged peptides rich in phosphoserine groups have been shown to create hydroxyapatite *in vitro* that was aligned in the same manner as observed in bone [36]. Injectable, crosslinked-alginate that can then mineralize *in situ* without the presence of other biological or chemical factors may present an advantage over pre-mineralized scaffolds or bone morphogenetic proteins in that it avoids adverse immune responses, limits systemic side effects, and is minimally-invasive for simple orthopaedic and reconstructive applications. However, in addition to hydroxyapatite formation and alignment, bone tissue engineering via mineralized alginate must also form constructs with high porosity and collagen content, osteo-conductive properties, bioactivity, and mechanical integrity in order for this method of repair to be feasible.

5. Conclusion

To understand the mechanism behind alginate calcification and to develop ways to regulate it, studies *in vitro* and *in viv*o were performed. Non-buffered calcium crosslinked alginate beads placed in a phosphate buffered bath sequestered the surrounding phosphate and calcified, forming traces of hydroxyapatite. Non-buffered calcium crosslinked alginate microbeads with or without ASCs also mineralized when implanted subcutaneously or intra-muscularly or injected subcutaneously after 1–6 months. More extensive analysis with microCT, FTIR, XRD, and EDS showed that the 1.6 ± 0.4 Ca/P ratio of the mineral formed closely matched hydroxyapatite found in bone. Incorporating bisphosphonate helped

regulate alginate calcification whereas using barium chloride as the crosslinking agent eliminated calcification. Buffering the crosslinking solution at pH 7.3 while washing and storing samples in basal media prior to implantation also eliminated calcification *in vivo*. This study effectively showed that calcium throughout the alginate is responsible for bulk hydroxyapatite formation and developed methods to partially regulate and eliminate alginate calcification.

Acknowledgments

This study was funded in part by the National Science Foundation Graduate Research Program (Lee), the Department of Defense, and Children's Healthcare of Atlanta. This research was also supported in part by NIH grant DE04141 (Boskey). The authors would like to thank Sha'Aqua Ashbury for her assistance with histology.

References

1. Leddy HA, Awad HA, Guilak F. Molecular diffusion in tissue-engineered cartilage constructs: effects of scaffold material, time, and culture conditions. J Biomed Mater Res B Appl Biomater. 2004; 70:397–406. [PubMed: 15264325]
2. Chang SC, Rowley JA, Tobias G, Genes NG, Roy AK, Mooney DJ, et al. Injection molding of chondrocyte/alginate constructs in the shape of facial implants. J Biomed Mater Res. 2001; 55:503–11. [PubMed: 11288078]
3. Hott ME, Megerian CA, Beane R, Bonassar LJ. Fabrication of tissue engineered tympanic membrane patches using computer-aided design and injection molding. Laryngoscope. 2004; 114:1290–5. [PubMed: 15235363]
4. Lee KY, Bouhadir KH, Mooney DJ. Controlled degradation of hydrogels using multi-functional cross-linking molecules. Biomaterials. 2004; 25:2461–6. [PubMed: 14751730]
5. Kong HJ, Kaigler D, Kim K, Mooney DJ. Controlling rigidity and degradation of alginate hydrogels via molecular weight distribution. Biomacromolecules. 2004; 5:1720–7. [PubMed: 15360280]
6. Boontheekul T, Kong HJ, Mooney DJ. Controlling alginate gel degradation utilizing partial oxidation and bimodal molecular weight distribution. Biomaterials. 2005; 26:2455–65. [PubMed: 15585248]
7. Hauselmann HJ, Fernandes RJ, Mok SS, Schmid TM, Block JA, Aydelotte MB, et al. Phenotypic stability of bovine articular chondrocytes after long-term culture in alginate beads. J Cell Sci. 1994; 107:17–27. [PubMed: 8175906]
8. Lim F, Sun AM. Microencapsulated islets as bioartificial endocrine pancreas. Science. 1980; 210:908–10. [PubMed: 6776628]
9. Alsberg E, Anderson KW, Albeiruti A, Franceschi RT, Mooney DJ. Cell-interactive alginate hydrogels for bone tissue engineering. J Dent Res. 2001; 80:2025–9. [PubMed: 11759015]
10. Rowley JA, Madlambayan G, Mooney DJ. Alginate hydrogels as synthetic extracellular matrix materials. Biomaterials. 1999; 20:45–53. [PubMed: 9916770]
11. Genes NG, Rowley JA, Mooney DJ, Bonassar LJ. Effect of substrate mechanics on chondrocyte adhesion to modified alginate surfaces. Arch Biochem Biophys. 2004; 422:161–7. [PubMed: 14759603]
12. Orive G, De Castro M, Kong HJ, Hernandez RM, Ponce S, Mooney DJ, et al. Bioactive cell–hydrogel microcapsules for cell-based drug delivery. J Control Release. 2009; 135:203–10. [PubMed: 19344677]
13. Chang SC, Tobias G, Roy AK, Vacanti CA, Bonassar LJ. Tissue engineering of autologous cartilage for craniofacial reconstruction by injection molding. Plast Reconstr Surg. 2003; 112:793–9. [PubMed: 12960860]
14. Vacanti CA, Bonassar LJ, Vacanti MP, Shuffiebarger J. Replacement of an avulsed phalanx with tissue-engineered bone. N Engl J Med. 2001; 344:1511–4. [PubMed: 11357154]
15. Goosen MF. Physico-chemical and mass transfer considerations in microencapsulation. Ann N Y Acad Sci. 1999; 875:84–104. [PubMed: 10415560]

16. Mierisch CM, Cohen SB, Jordan LC, Robertson PG, Balian G, Diduch DR. Transforming growth factor-beta in calcium alginate beads for the treatment of articular cartilage defects in the rabbit. Arthroscopy. 2002; 18:892–900. [PubMed: 12368788]
17. Paek HJ, Campaner AB, Kim JL, Aaron RK, Ciombor DM, Morgan JR, et al. In vitro characterization of TGF-beta1 release from genetically modified fibro-blasts in Ca(2+)-alginate microcapsules. ASAIO J. 2005; 51:379–84. [PubMed: 16156303]
18. Robitaille R, Pariseau JF, Leblond FA, Lamoureux M, Lepage Y, Halle JP. Studies on small (<350 microm) alginate-poly-L-lysine microcapsules. III. Biocompatibility of smaller versus standard microcapsules. J Biomed Mater Res. 1999; 44:116–20. [PubMed: 10397911]
19. Klokk TI, Melvik JE. Controlling the size of alginate gel beads by use of a high electrostatic potential. J Microencapsul. 2002; 19:415–24. [PubMed: 12396380]
20. Thornton AJ, Alsberg E, Hill EE, Mooney DJ. Shape retaining injectable hydrogels for minimally invasive bulking. J Urol. 2004; 172:763–8. [PubMed: 15247778]
21. Ma HL, Chen TH, Low-Tone Ho L, Hung SC. Neocartilage from human mesenchymal stem cells in alginate: implied timing of transplantation. J Biomed Mater Res A. 2005; 74:439–46. [PubMed: 16013059]
22. Davey RB, Sparnon AL, Byard RW. Unusual donor site reactions to calcium alginate dressings. Burns. 2000; 26:393–8. [PubMed: 10751708]
23. Bhopatkar D, Anal AK, Stevens WF. Ionotropic alginate beads for controlled intestinal protein delivery: effect of chitosan and barium counter-ions on entrapment and release. J Microencapsul. 2005; 22:91–100. [PubMed: 16019894]
24. Blumenthal NC. Mechanisms of inhibition of calcification. Clin Orthop Relat Res. 1989:279–89. [PubMed: 2676300]
25. Nancollas GH, Johnsson MA. Calculus formation and inhibition. Adv Dent Res. 1994; 8:307–11. [PubMed: 7865091]
26. Zuk PA, Zhu M, Ashjian P, De Ugarte DA, Huang JI, Mizuno H, et al. Human adipose tissue is a source of multipotent stem cells. Mol Biol Cell. 2002; 13:4279–95. [PubMed: 12475952]
27. Boyan, BD.; Kinney, RC.; Schwartz, Z. Microencapsulation of cells in hydrogels using electrostatic potentials. U.S.P.a.T. Office; United States: 2008. p. 1-11.
28. Ranly DM, McMillan J, Keller T, Lohmann CH, Meunch T, Cochran DL, et al. Platelet-derived growth factor inhibits demineralized bone matrix-induced intramuscular cartilage and bone formation. A study of immunocompromised mice. J Bone Joint Surg Am. 2005; 87:2052–64. [PubMed: 16140821]
29. Boyan BD, Wong KL, Wang L, Yao H, Guldberg RE, Drab M, et al. Regulation of growth plate chondrocytes by 1,25-dihydroxyvitamin D3 requires caveolae and caveolin-1. J Bone Miner Res. 2006; 21:1637–47. [PubMed: 16995819]
30. Rubin J, Schwartz Z, Boyan BD, Fan X, Case N, Sen B, et al. Caveolin-1 knockout mice have increased bone size and stiffness. J Bone Miner Res. 2007; 22:1408–18. [PubMed: 17550335]
31. Dallas CE, Williams PL. Barium: rationale for a new oral reference dose. J Toxicol Environ Health B Crit Rev. 2001; 4:395–429. [PubMed: 11695044]
32. Recker RR, Lewiecki EM, Miller PD, Reiffel J. Safety of bisphosphonates in the treatment of osteoporosis. Am J Med. 2009; 122:S22–32. [PubMed: 19187809]
33. Yao S, McCarthy PL, Dunford LM, Roy DM, Brown K, Paplham P, et al. High prevalence of early-onset osteopenia/osteoporosis after allogeneic stem cell transplantation and improvement after bisphosphonate therapy. Bone Marrow Transplant. 2008; 41:393–8. [PubMed: 17994116]
34. Baicu SC, Taylor MJ. Acid–base buffering in organ preservation solutions as a function of temperature: new parameters for comparing buffer capacity and efficiency. Cryobiology. 2002; 45:33–48. [PubMed: 12445548]
35. Bonewald LF, Harris SE, Rosser J, Dallas MR, Dallas SL, Camacho NP, et al. von Kossa staining alone is not sufficient to confirm that mineralization in vitro represents bone formation. Calcif Tissue Int. 2003; 72:537–47. [PubMed: 12724828]
36. Hartgerink JD, Beniash E, Stupp SI. Self-assembly and mineralization of peptide-amphiphile nanofibers. Science. 2001; 294:1684–8. [PubMed: 11721046]

37. Tomazic BB. Physiochemical principles of cardiovascular calcification. Z Kardiol. 2001; 90:68–80. [PubMed: 11374037]

38. Crowell JA, Bowers GN Jr. Apparent binding of ionized calcium by various buffers. Clin Chem. 1985; 31:267–70. [PubMed: 3967360]

39. Kakudo N, Shimotsuma A, Miyake S, Kushida S, Kusumoto K. Bone tissue engineering using human adipose-derived stem cells and honeycomb collagen scaffold. J Biomed Mater Res A. 2008; 84:191–7. [PubMed: 17607760]

40. Grellier M, Granja PL, Fricain JC, Bidarra SJ, Renard M, Bareille R, et al. The effect of the co-immobilization of human osteoprogenitors and endothelial cells within alginate microspheres on mineralization in a bone defect. Biomaterials. 2009; 30:3271–8. [PubMed: 19299013]

41. Mann S, Archibald DD, Didymus JM, Douglas T, Heywood BR, Meldrum FC, et al. Crystallization at inorganic–organic interfaces: biominerals and biomimetic synthesis. Science. 1993; 261:1286–92. [PubMed: 17731856]

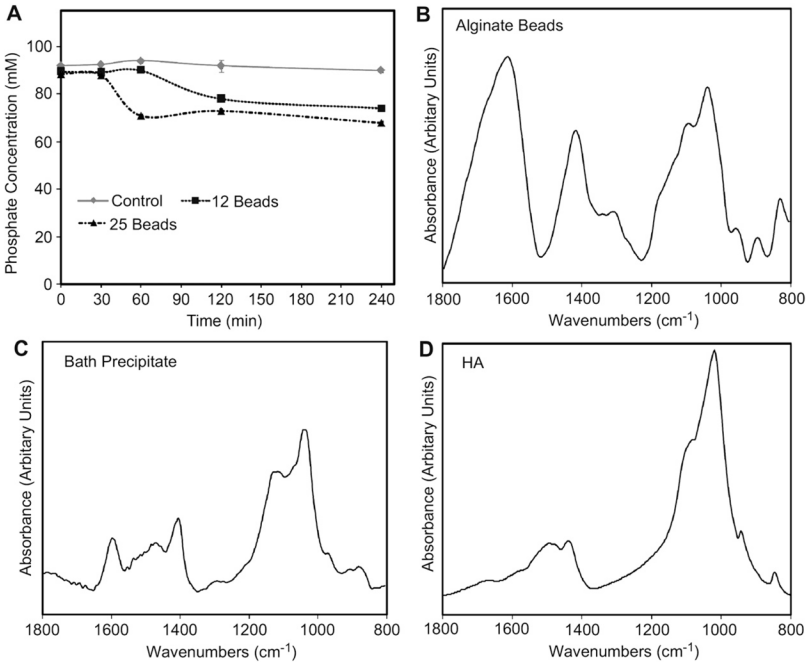

Fig. 1.

In vitro study. (A) Phosphate concentration of buffered bath over time for different amounts of alginate added to 25 ml of 4 mM $(NH_4)_2HPO_4$ in 0.05 M Tris buffer at pH 7.4 ($n = 3$ for each experimental group and time). FTIR spectra of (B) lyophilized alginate beads, (C) precipitate from the bath, and (D) pure hydroxyapatite.

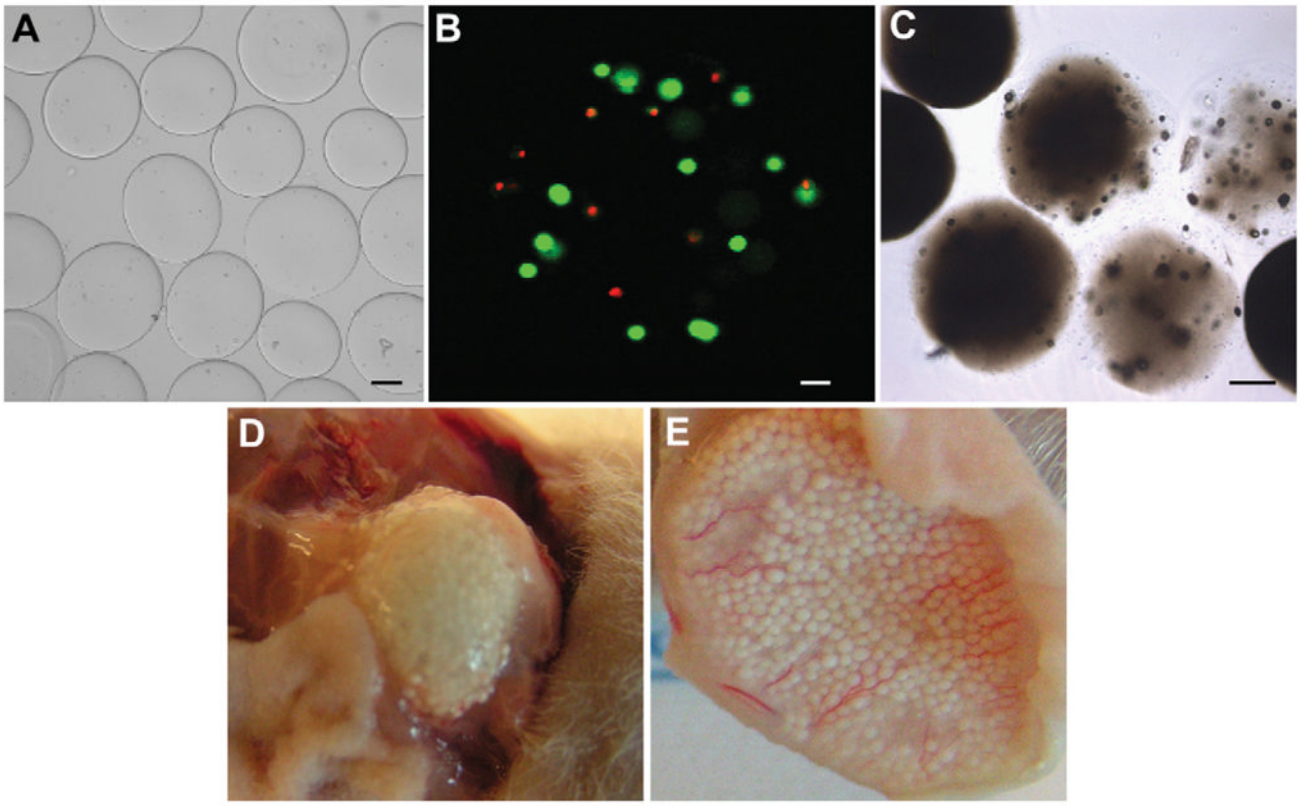

Fig. 2.

Gross-visualization of alginate microbead mineralization. (A) Microbeads before implantation or injection under a light microscope (Bar = 100 μm). (B) Live/dead staining of human ASCs within a single microbead post-injection (Bar = 25 μm) (C) Visualization of mineralized microbeads 3 months post-implantation under a light microscope (Bar = 100 μm). (D) Mineralized microbeads 3 months post-implantation. (E) Mineralized microbeads 1 month post-injection.

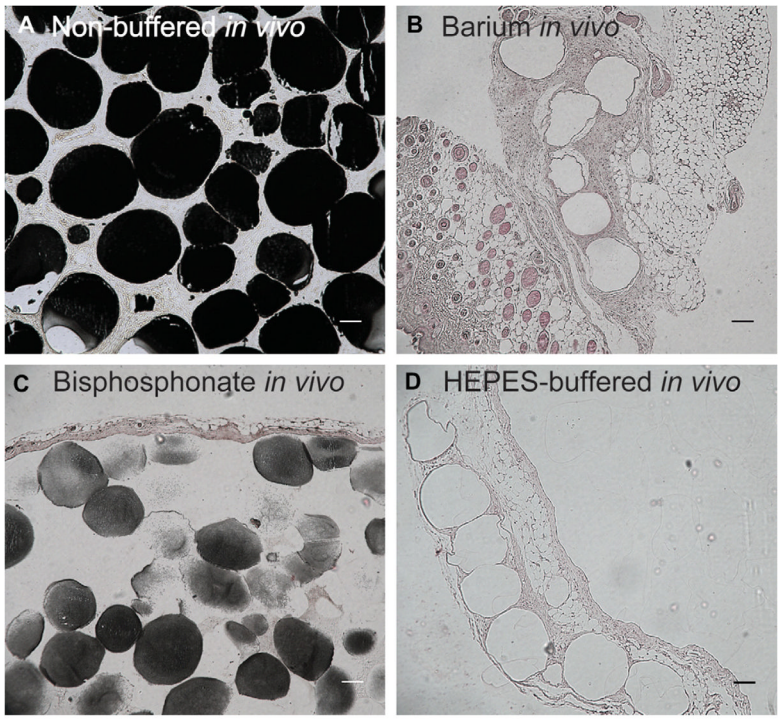

Fig. 3.

Histology of *in vivo* microbeads. von Kossa with nuclear fast red counter stain to determine calcification for representative (A) non-buffered, (B) barium chloride, (C), bisphosphonate, (D) buffered samples *in vivo* after 2 months. Bar represents 100 μm for all images.

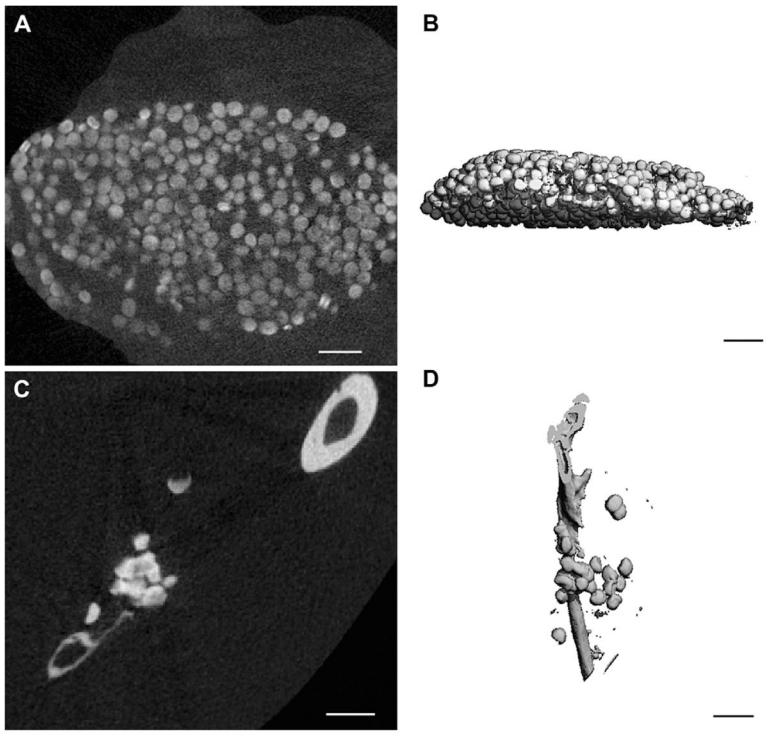

Fig. 4.

MicroCT analysis of non-buffered *in vivo* samples. (A) Representative X-ray cross-section of subcutaneously implanted non-buffered microbeads after 5 weeks *in vivo*. (B) 3-D reconstruction of subcutaneously implanted non-buffered microbeads after 5 weeks *in vivo*. (C) Representative sagittal X-ray cross-section of intramuscularly implanted non-buffered microbeads near the tibia after 5 weeks *in vivo*. (D) 3-D reconstruction of intramuscular implanted non-buffered microbeads along with the tibia after 5 weeks *in vivo*. Bar represents 1 mm for all images.

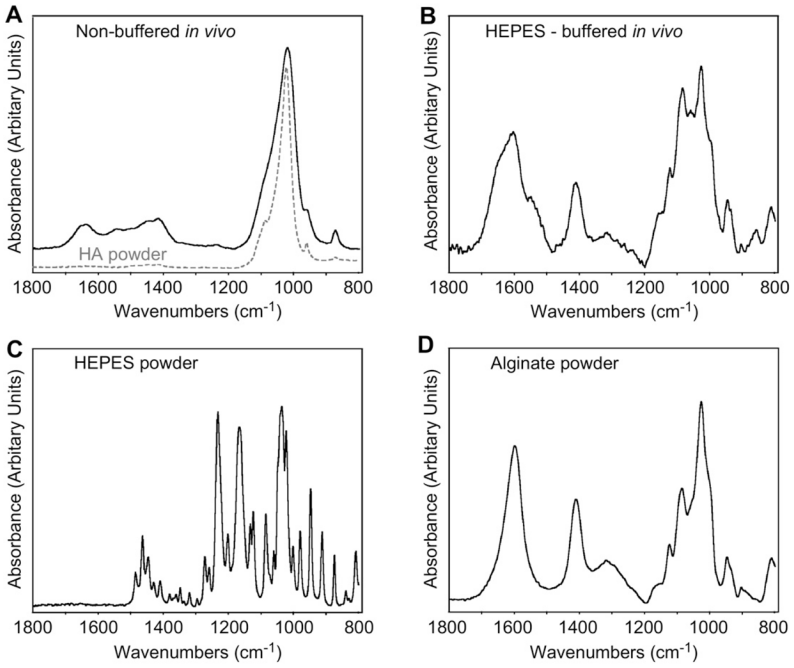

Fig. 5.

FTIR. Spectra of (A) non-buffered microbeads after 5 weeks *in vivo*, (B) buffered microbeads after 5 weeks *in vivo*, (C) HEPES powder used to buffer the crosslinking solution, and (D) alginate powder used to make the microbeads.

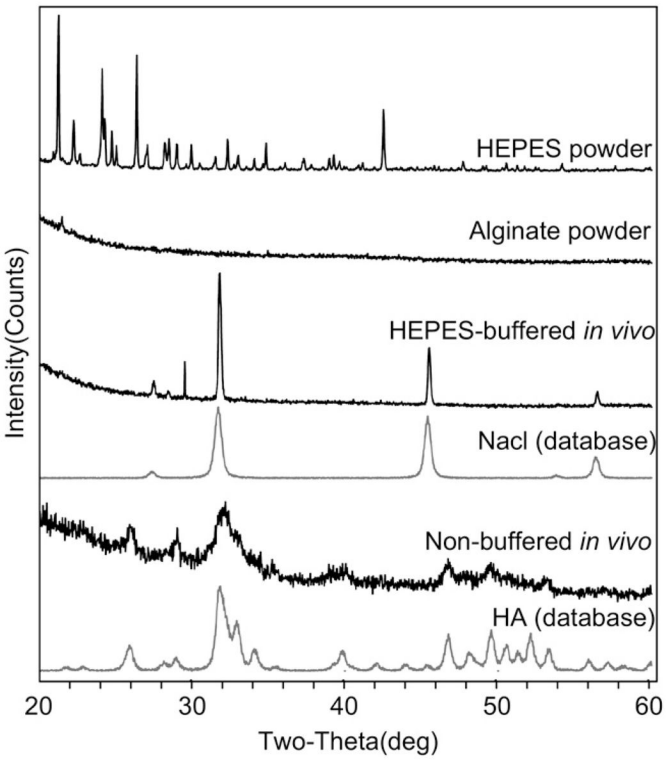

Fig. 6.

XRD. Spectra of HEPES powder used to buffer the crosslinking solution, alginate powder used to make the microbeads, buffered microbeads after 5 weeks *in vivo*, NaCl from the database, non-buffered microbeads after 5 weeks *in vivo*, and hydroxyapatite from the database.

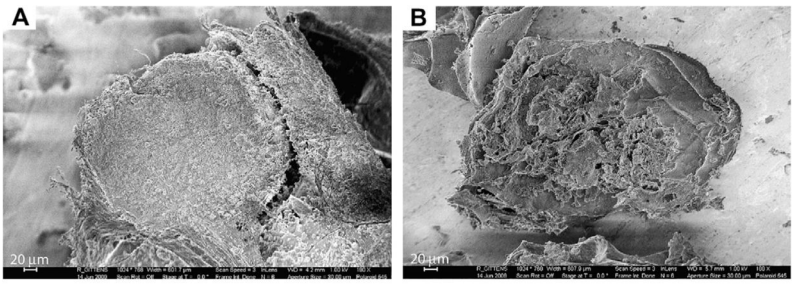

Fig. 7.
SEM Images. (A) Lyophilized non-buffered microbeads after 5 weeks *in vivo*. (B) Lyophilized buffered microbeads after 5 weeks *in vivo*.

Table 1

Mineralization of cellular and acellular microbeads in male nude mice with different delivery methods at different times subcutaneously based on visual inspection.

Months Post Op	Empty	ASC-seeded
1	*Implantation*: 4/4 Mineralized	*Implantation*: 4/4 Mineralized
	Injection: 3/4 Mineralized[a]	*Injection*: 3/4 Mineralized
3	*Implantation*: 4/4 Mineralized	*Implantation*: 4/4 Mineralized
	Injection: 3/4 Mineralized[a]	*Injection*: 4/4 Mineralized
6	*Implantation*: 4/4 Mineralized	*Implantation*: 4/4 Mineralized
	Injection: 4/4 Mineralized	*Injection*: 4/4 Mineralized

[a]Microbeads for one sample disappeared and had no volume retention.

Table 2

Attempts to regulating calcification by modifying the crosslinking solution and delivery location 5–8 weeks post-implantation or injection based on von Kossa staining.

	Non-buffered	**Barium**	**Bisphosphonate**	**HEPES-Buffered**
Implantation	*Subcutaneous*: 4/4 Calcified	–	–	*Subcutaneous*: 0/4 Calcified
	Intramuscular: 4/6 Calcified	–	–	*Intramuscular*: 0/4 Calcified
Injection	–	0/4 Calcified	2/4 Calcified	0/4 Calcified

Table 3

EDS calculated elemental composition of non-buffered and buffered *in vivo* samples.

	Concentration [atomic %][a,b]									
	C	**O**	**Na**	**Mg**	**Al**	**P**	**S**	**Cl**	**Ca**	**K**
Non-buffered	34.0 ± 4.3	47.2 ± 2.0	<1	<1	1.2 ± 0.4	6.3 ± 0.8	<1	–	10.2 ± 1.3	–
HEPES-buffered	41.6 ± 1.0	27.5 ± 1.9	14.3 ± 0.7	–	<1	1.15 ± 0.1	<1	13.2 ± 1.8	<1	<1

[a] The values should be evaluated with an error of approximately ± 2% relative.

[b] Elements that were not present in all measurements of the same sample were not included in the table (e.g., Si).